Acta Crystallographica Section D
Biological Crystallography
ISSN 1399-0047

Structural and biochemical analyses of the *Streptococcus pneumoniae* L,D-carboxypeptidase DacB

Juan Zhang,‡ Yi-Hu Yang,‡ Yong-Liang Jiang,* Cong-Zhao Zhou and Yuxing Chen*

Hefei National Laboratory for Physical Sciences at the Microscale and School of Life Sciences, University of Science and Technology of China, Hefei 230027, People's Republic of China

‡ These authors contributed equally to this work.

Correspondence e-mail: jyl@mail.ustc.edu.cn, cyxing@ustc.edu.cn

Received 27 May 2014
Accepted 19 November 2014

PDB reference: DacB, 4nt9

The L,D-carboxypeptidase DacB plays a key role in the remodelling of *Streptococcus pneumoniae* peptidoglycan during cell division. In order to decipher its substrate-binding properties and catalytic mechanism, the 1.71 Å resolution crystal structure of DacB from *S. pneumoniae* TIGR4 is reported. Structural analyses in combination with comparisons with the recently reported structures of DacB from *S. pneumoniae* D39 and R6 clearly demonstrate that DacB adopts a zinc-dependent carboxypeptidase fold and belongs to the metallopeptidase M15B subfamily. In addition, enzymatic activity assays further confirm that DacB indeed acts as an L,D-carboxypeptidase towards the tetrapeptide L-Ala-D-iGln-L-Lys-D-Ala of the peptidoglycan stem, with K_m and k_{cat} values of 2.84 ± 0.37 m*M* and 91.49 ± 0.05 s^{-1}, respectively. Subsequent molecular docking and site-directed mutagenesis enable the assignment of the key residues that bind to the tetrapeptide. Altogether, these findings provide structural insights into substrate recognition in the metallopeptidase M15B subfamily.

1. Introduction

Peptidoglycan (PG) is an important component of the bacterial cell wall that maintains osmotic stability and determines the shape of bacteria (Zapun *et al.*, 2008). It is composed of glycan chains with alternating β-1,4-linked *N*-acetylglucosamine (GlcNAc) and *N*-acetylmuramic acid (MurNAc) residues, in addition to cross-linked stem peptides (Scheffers & Pinho, 2005). The growth of PG involves not only synthesis by PG synthases, but also remodelling by a series of hydrolases (Vollmer, Joris *et al.*, 2008). These PG hydrolases play key roles throughout the life cycle of bacteria, including cell growth, shape maintenance, daughter-cell separation, PG maturation and cell-wall fragment recycling (Wyckoff *et al.*, 2012). According to the specificity towards various covalent bonds, these PG hydrolases have been classified into several groups: glycosidases that hydrolyze β-1,4 bonds between sugars, peptidases that cleave short peptides (carboxypeptidases) or peptide cross-bridges (endopeptidases), and *N*-acetylmuramoyl-L-alanine amidases (amidases for short) that separate peptides from sugar strands (Vollmer, Blanot *et al.*, 2008).

PG hydrolases have been systematically studied in rod-shaped bacterial models such as *Bacillus subtilis* and *Escherichia coli* (Smith *et al.*, 2000; van Heijenoort, 2011). Recently, the PG-degradation machinery of the ovococcal-shaped human pathogen *Streptococcus pneumoniae* has been systematically explored (Massidda *et al.*, 2013; Sham *et al.*, 2012). To date, 13 genes in the *S. pneumoniae* genome have been annotated to encode proteins involved in PG hydrolysis (Barendt *et al.*, 2011; Sham *et al.*, 2012). Single deletion of

several genes (*dacA*, *dacB*, *pcsB*, *pmp23* and *spd_0703*) leads to aberrant cell division and morphology, indicating that the proteins encoded by these genes are involved in PG remodelling (Barendt *et al.*, 2011). In addition, mutation of either *dacA* or *dacB* leads to similar morphological defects, including heterogeneity in cell size and shape and misplaced division septa (Schuster *et al.*, 1990; Barendt *et al.*, 2011). DacA, also known as penicillin-binding protein 3 (PBP3; Hakenbeck & Kohiyama, 1982), acts as a D,D-carboxypeptidase that cleaves the pentapeptide L-Ala-D-iGln-L-Lys-D-Ala-D-Ala (Severin *et al.*, 1992; Morlot *et al.*, 2005). The tetrapeptide L-Ala-D-iGln-L-Lys-D-Ala produced by DacA was proposed to be further cleaved by DacB to generate the tripeptide L-Ala-D-iGln-L-Lys (Barendt *et al.*, 2011). Moreover, DacA and DacB may regulate PG cross-linking by limiting the amount and the location of the full-length PG pentapeptides (Morlot *et al.*, 2004; Barendt *et al.*, 2011).

Comparing the composition of the peptidoglycan peptides from the *dacB*-knockout *S. pneumoniae* D39 strain with that from the wild-type strain, the amount of tetrapeptide increases whereas the amount of tripeptide decreases, indicating that DacB is an L,D-carboxypeptidase that hydrolyzes the peptide bond between L-Lys and D-Ala (Barendt *et al.*, 2011; Abdullah *et al.*, 2014). The L,D-carboxypeptidase activity of DacB from *S. pneumoniae* R6 (termed *Sp*LdcB) is further confirmed by *in vitro* enzymatic assays using peptidoglycan from the *ldcB*-knockout strain and the synthetic tetrapeptide L-Ala-D-Gln-L-Lys-D-Ala (Hoyland *et al.*, 2014). Recently reported DacB structures from *S. pneumoniae* D39 and R6 reveal that the overall structure resembles the members of the M15B subfamily, which consist of a central β-sheet surrounded by several helices. The active-site zinc ion is tetrahedrally coordinated by a couple of conserved residues (Abdullah *et al.*, 2014; Hoyland *et al.*, 2014). In addition, the structure of *Sp*LdcB in complex with a product mimic led to the assignment of key residues essential for peptidoglycan recognition and catalysis (Hoyland *et al.*, 2014). Notably, the structure of another member of the M15B subfamily, the D,D-dipeptidase/D,D-carboxypeptidase VanXY, has recently been reported (Meziane-Cherif *et al.*, 2014). Despite a similar core structure, DacB presents a larger active-site pocket compared with VanXY resulting from the absence of the bisubstrate selectivity loop (Abdullah *et al.*, 2014; Hoyland *et al.*, 2014; Meziane-Cherif *et al.*, 2014).

Here, we report the 1.71 Å resolution crystal structure of DacB from *S. pneumoniae* TIGR4 and detect its L,D-carboxypeptidase activity towards the tetrapeptide L-Ala-D-iGln-L-Lys-D-Ala. The structure closely resembles the reported DacB structures, with a tetrahedrally coordinated active-site zinc ion (Abdullah *et al.*, 2014; Hoyland *et al.*, 2014). Our enzymatic assays also confirm that DacB is indeed an L,D-carboxypeptidase, which is consistent with previous results (Hoyland *et al.*, 2014). Moreover, molecular docking together with site-directed mutagenesis enables us to clearly identify key residues for substrate recognition and catalysis. Structural comparison of DacB with VanXY reveals distinct features of the active-site pocket which might be involved in substrate specificity. These findings increase our understanding of the substrate recognition and catalysis of the M15B subfamily peptidases and might help in the design of novel anti-streptococcal drugs.

2. Materials and methods

2.1. Cloning, expression and purification of DacB and mutants

The coding sequence of DacB/SP_0629 (residues Glu27–Asp238), excluding the signal peptide, was amplified from genomic DNA of *S. pneumoniae* TIGR4 using the primers DacB-sense (5′-ACACATATGGAAGATGGAGAAACTA-AGACA-3′) and DacB-anti (5′-ACTCTCGAGTTAATCG-ACGTAGTCTCCGCC-3′). The DNA fragment was cloned into the NdeI/XhoI sites of a pET-28a-derived vector with an N-terminal hexahistidine tag. The construct was transformed into *E. coli* strain BL21 (DE3) (Novagen) cultured in LB culture medium (10 g NaCl, 10 g Bacto tryptone and 5 g yeast extract per litre). The cells were grown at 37°C to an $OD_{600\ nm}$ of 0.6. Expression of the recombinant protein was induced with 0.2 m*M* isopropyl β-D-1-thiogalactopyranoside (IPTG) for a further 20 h at 16°C before harvesting. The cells were collected and resuspended in 30 ml lysis buffer (20 m*M* Tris–HCl pH 8.8, 100 m*M* NaCl). After 2.5 min of sonication and centrifugation at 12 000*g* for 30 min, the supernatant containing the target protein was collected and loaded onto an Ni–NTA column (GE Healthcare) equilibrated with binding buffer (20 m*M* Tris–HCl pH 8.0, 100 m*M* NaCl). The target protein was eluted with buffer consisting of 20 m*M* Tris–HCl pH 8.0, 100 m*M* NaCl, 500 m*M* imidazole and further loaded onto a Superdex 75 column (GE Healthcare) pre-equilibrated with binding buffer. The apparent molecular weight of DacB is 24.5 kDa as shown by size-exclusion chromatography on a Superdex 75 column. The protein standards were bovine serum albumin, ovalbumin, chymotrypsinogen A, myoglobulin and ribonuclease A, which have molecular masses of 67, 44, 25, 17 and 13.7 kDa, respectively. Fractions containing the target protein were pooled and concentrated to 17 mg ml^{-1} for crystallization. The protein concentration was measured using absorbance spectroscopy at 280 nm (OD-1000 Spectrophotometer, One Drop). Protein samples in the peak fractions were collected without concentration for enzymatic activity assays. The purity of the protein was assessed by electrophoresis and the protein samples were stored at −80°C.

Site-directed mutagenesis was performed using the QuikChange site-directed mutagenesis kit (Stratagene, La Jolla, California, USA) with the plasmid encoding wild-type DacB as the template. The mutants were expressed, purified and stored in the same manner as the wild-type protein.

Selenomethionine (SeMet)-labelled DacB protein was expressed in *E. coli* strain B834 (DE3) (Novagen). Transformed cells were grown at 37°C in SeMet medium (M9 medium with 25 µg ml^{-1} SeMet and other essential amino acids at 50 µg ml^{-1}) containing 30 µg ml^{-1} kanamycin until the $OD_{600\ nm}$ reached about 0.6. Expression of the protein was

then induced with 0.2 m*M* IPTG for 20 h at 16°C. SeMet-substituted His_6-DacB was purified in the same manner as native His_6-DacB.

2.2. Crystallization, data collection and processing

Both native and SeMet-substituted DacB were concentrated to 17 mg ml^{-1} by ultrafiltration (Millipore Amicon) for crystallization. Screening for crystallization conditions was performed using the Crystal Screen, Crystal Screen 2, Index, Grid Screens, Complex Screens and SaltRx kits (Hampton Research). Crystals of native and SeMet-substituted DacB were grown at 25°C using the sitting-drop vapour-diffusion method, with the initial condition consisting of mixing 1 µl protein sample with an equal volume of precipitant solution consisting of 0.2 *M* sodium acetate, 0.1 *M* Tris–HCl pH 8.5, 30%(*w*/*v*) polyethylene glycol (PEG) 4000. Typically, crystals appeared in about two weeks and reached maximum size in one month. The crystals were transferred to cryoprotectant consisting of reservoir solution supplemented with 25%(*v*/*v*) glycerol and were then flash-cooled with liquid nitrogen. Both native data and SeMet-derivative data were collected from a single crystal at 100 K in a nitrogen-gas stream using an MX225 CCD (MAR Research, Germany) on beamline 17U at the Shanghai Synchrotron Radiation Facility (SSRF). The data were collected at wavelengths of 0.97892 Å for the native crystal and 0.97923 Å for the SeMet-derivative crystal. All diffraction data were integrated and scaled with *HKL*-2000 (Otwinowski & Minor, 1997).

2.3. Structure determination, refinement and docking

The crystal structure of DacB was determined by the single-wavelength anomalous dispersion (SAD) phasing technique (Brodersen *et al.*, 2000) from a single SeMet-substituted protein crystal to a maximum resolution of 2.12 Å. The *AutoSol* program from *PHENIX* (Adams *et al.*, 2010) was used to locate the Se atoms and to calculate the initial phases, yielding FOM and BAYES-CC values of 0.326 and 36.08, respectively. Each asymmetric unit contains one DacB molecule. The initial electron-density maps showed clear features of secondary-structural elements, permitting the building of approximately half of the structure in *PHENIX*, yielding a model CC of 0.50. Automatic model building was carried out using the initial structure as a starting point with *Buccaneer* (Cowtan, 2006) and *AutoBuild* in *PHENIX*. The initial model was refined with *REFMAC*5 (Murshudov *et al.*, 2011) as part of the *CCP*4 (Winn *et al.*, 2011) program suite and rebuilt interactively using *Coot* (Emsley & Cowtan, 2004). The model was used as the search model against the 1.71 Å resolution native data by molecular replacement using *MOLREP* (Vagin & Teplyakov, 2010) as part of the *CCP*4 (Winn *et al.*, 2011) program suite. The final model consisting of three molecules in an asymmetric unit was refined using *phenix.refine* (Afonine *et al.*, 2012) and *Coot* without NCS restraints. The final model was evaluated with *MolProbity* (Chen *et al.*, 2010) and *PROCHECK* (Laskowski *et al.*, 1993). Crystallographic parameters, data-collection statistics and refinement statistics are listed in Table 1. The secondary structure was assigned by *ESPript* (http://espript.ibcp.fr). Structural superposition was performed by *Superpose Molecules* as implemented in *CCP*4. The docking of the tetrapeptide to the structure of DacB was performed with *AutoDock Vina* (v.1.0; Trott & Olson, 2010), which uses a unique algorithm that implements a machine-learning approach in its scoring function. The docking allowed a population of possible conformations and orientations for the ligand at the binding site to be obtained. Using *AutoDock Tools* v.1.5.4 (Morris *et al.*, 2009), polar H atoms were added to

Table 1
Crystal parameters, data collection and structure refinement.

Values in parentheses are for the highest resolution bin.

	SeMet DacB	DacB
Data collection		
Space group	$P3_221$	$P2_1$
Wavelength (Å)	0.97923	0.97892
Unit-cell parameters		
a (Å)	66.07	55.11
b (Å)	66.07	68.08
c (Å)	111.05	80.35
α (°)	90.00	90.00
β (°)	90.00	108.41
γ (°)	120.00	90.00
Resolution range (Å)	50.00–2.12 (2.41–2.12)	47.47–1.71 (1.80–1.71)
Unique reflections	16450 (1037)	58226 (7290)
Completeness (%)	99.9 (99.7)	94.8 (81.9)
$\langle I/\sigma(I)\rangle$	19.2 (3.4)	8.8 (2.0)
$R_{\rm merge}$†	0.194 (0.924)	0.090 (0.684)
$R_{\rm p.i.m}$	0.045 (0.270)	0.056 (0.427)
$R_{\rm meas}/R_{\rm r.i.m}$	0.199 (0.966)	0.106 (0.809)
$CC_{1/2}$	0.995 (0.947)	0.996 (0.695)
Wilson B factor (Å^2)	32.1	17.0
Average multiplicity	18.3 (16.2)	3.5 (3.5)
Phasing statistics		
Anomalous $R_{\rm merge}$	0.187 (0.900)	
Anomalous multiplicity	9.8 (6.0)	
FOM	0.326	
BAYES-CC	36.08	
Model-CC	0.50	
Structure refinement		
Resolution range (Å)		47.47–1.71
R factor‡/$R_{\rm free}$§		0.17/0.21
No. of protein atoms		4401
No. of water atoms		396
No. of Zn^{2+} ions		3
No. of acetate molecules		3
R.m.s.d.¶, bond lengths (Å)		0.01
R.m.s.d., bond angles (°)		1.37
Mean B factor (Å^2)		23.4
Individual B factors (Å^2)		
Zinc ions		18.7, 16.3, 18.6
Acetate molecules		24.2, 20.8, 22.7
Validation statistics		
Poor rotamers (%)		1.13
Clashscore		3.82
Ramachandran plot†† (%)		
Most favoured		98.2
Additionally allowed		1.8
Outliers		0
PDB entry		4nt9

† $R_{\rm merge} = \sum_{hkl}\sum_i |I_i(hkl) - \langle I(hkl)\rangle|/\sum_{hkl}\sum_i I_i(hkl)$, where $I_i(hkl)$ is the intensity of an observation and $\langle I(hkl)\rangle$ is the mean value for its unique reflection; summations are over all reflections. ‡ R factor = $\sum_{hkl}\big||F_{\rm obs}| - |F_{\rm calc}|\big|/\sum_{hkl}|F_{\rm obs}|$, where $|F_{\rm obs}|$ and $|F_{\rm calc}|$ are the observed and calculated structure-factor amplitudes, respectively. § $R_{\rm free}$ was calculated with 5% of the data excluded from the refinement. ¶ Root-mean-square deviation from ideal values (Engh & Huber, 1991). †† Categories were defined by *MolProbity* (Chen *et al.*, 2010).

the DacB structure and its nonpolar H atoms were merged. The protein and ligand were converted from PDB format to PDBQT format. All single bonds within the tetrapeptide were set to allow rotation. A grid box covering the entire substrate-binding site was used to place the tetrapeptide freely. The results were sorted by predicted binding affinity and visually analyzed using *PyMOL* (http://www.pymol.org/).

2.4. Determination of the active-site metal

Atomic absorption spectroscopy (Atomscan Advantage, Thermo Ash Jarell Corporation, USA) was used to determine the metal content. The purified DacB in buffer consisting of 20 m*M* Tris–HCl pH 8.0, 100 m*M* NaCl was concentrated to 30 mg ml^{-1} and used for analysis.

2.5. Enzymatic activity assays

The synthetic peptides L-Ala-D-iGln-L-Lys-D-Ala-D-Ala, Ac-L-Lys-D-Ala-D-Ala, D-Ala-D-Ala, L-Ala-D-iGln-L-Lys-D-Ala, D-iGln-L-Lys-D-Ala and Ac-L-Lys-D-Ala were purchased from GL Biochem, Shanghai. Peptide samples were dissolved in double-distilled water at a concentration of 100 m*M* and stored at −80°C. Protein samples for enzymatic activity assays

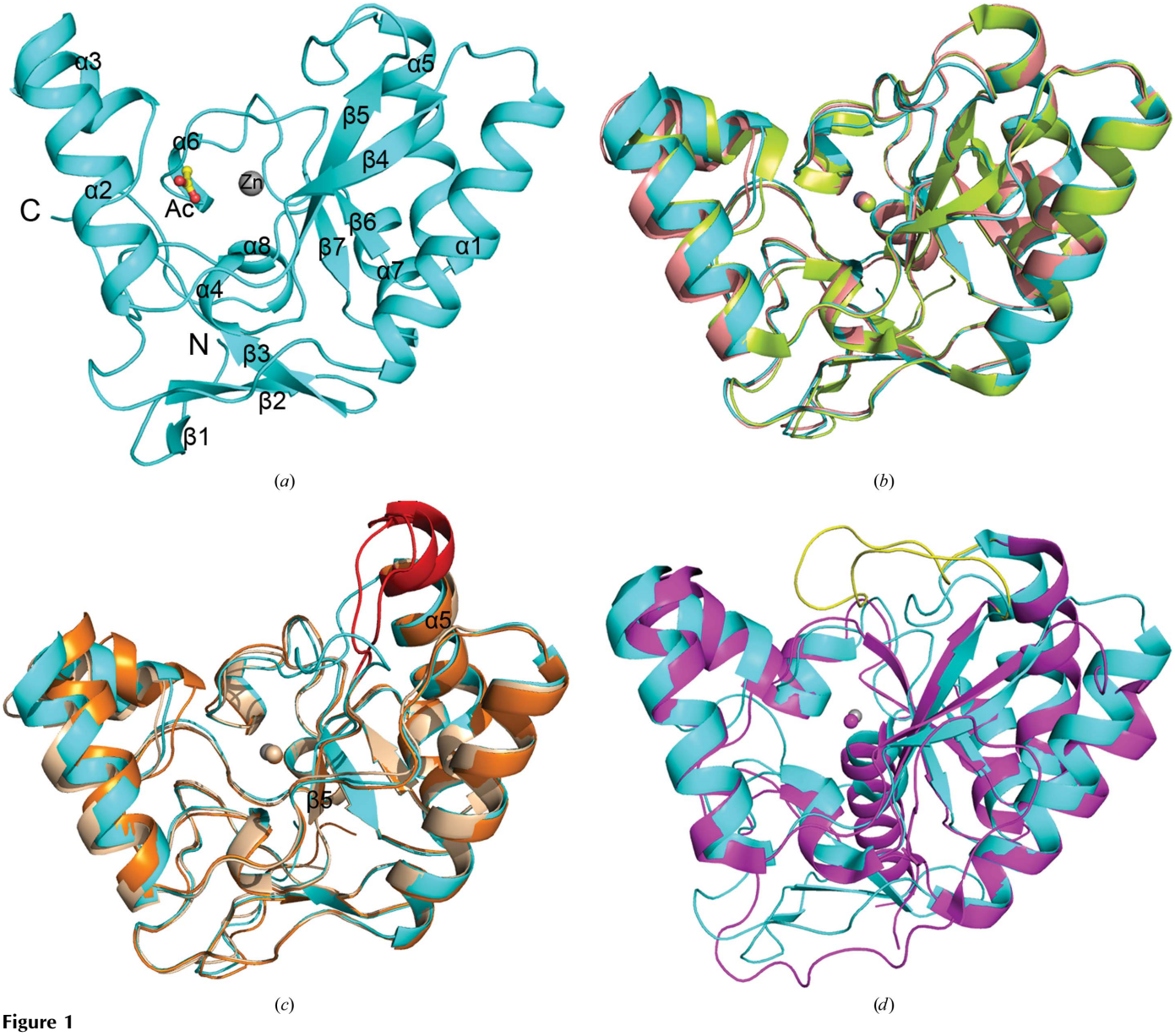

Figure 1
The overall structure of DacB. (*a*) A cartoon representation of the DacB structure. The zinc ion in the active site is shown as a grey sphere and the acetate molecule is shown as yellow sticks. (*b*) Superposition of DacB from *S. pneumoniae* TIGR4 on chain *A* of DacB from *S. pneumoniae* D39 (salmon; PDB entry 4d0y) and *Sp*LdcB in complex with D-Ala (lemon; PDB entry 4ox5). (*c*) Superposition of DacB from *S. pneumoniae* TIGR4 on chain *B* of DacB from *S. pneumoniae* D39 (wheat; PDB entry 4d0y) and *Sp*LdcB in complex with a product mimic (orange; PDB entry 4oxd). The rearrangements of the *β*5–*α*5 loop and N-terminus of helix *α*5 are highlighted as red cartoons. (*d*) Superposition of DacB from *S. pneumoniae* TIGR4 on the vancomycin-resistance bifunctional D,D-dipeptidase/D,D-carboxypeptidase VanXY$_C$ from *E. gallinarum* (magenta; PDB entry 4oak). The bisubstrate selectivity loop in VanXY$_C$ is coloured yellow.

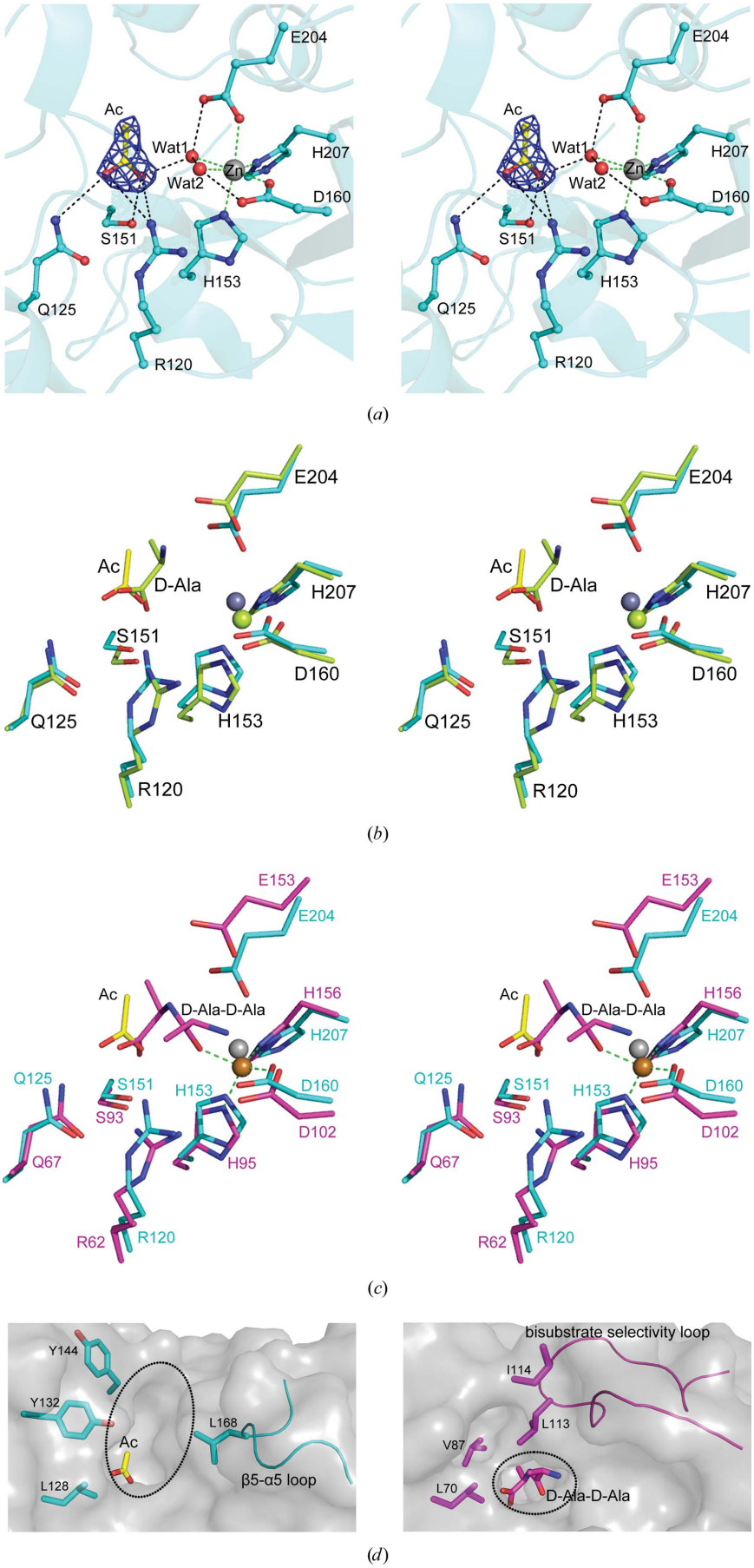

were collected without concentration and were stored at −80°C with the addition of glycerol to a final concentration of 50%(*v*/*v*). The enzymatic activities of wild-type DacB towards different peptides were detected at 37°C in a 30 µl system containing buffer consisting of 100 m*M* Tris–HCl pH 7.5. The reactions were initiated by the addition of DacB enzyme and were terminated by adding 0.1 *M* HCl after 15 min. An assay mixture without any enzyme was used as a control. The hydrolysis of peptides was measured by high-performance liquid chromatography (HPLC; Agilent 1200 series). The column (Eclipse XDB-C18 column, 4.6 × 150 mm, Agilent) was equilibrated using buffer consisting of 2% acetonitrile and 0.1% trifluoroacetic acid. Samples with a 10 µl volume were injected and separated at a flow rate of 1 ml min^{-1} with a mobile phase consisting of 2% acetonitrile containing 0.1% trifluoroacetic acid. The decrease in substrate was monitored by the absorbance at 220 nm. To determine the enzymatic parameters towards L-Ala-D-iGln-L-Lys-D-Ala, D-iGln-L-Lys-D-Ala and Ac-L-Lys-D-Ala, the enzyme concentrations were maintained at 10, 10 and 150 n*M*, respectively, whereas the substrate concentrations varied in the ranges 0.2–10, 0.5–20 and 0.5–20 m*M*, respectively. The decrease in substrates was calculated based on peptide standards quantified using a series of concentrations ranging from 0.5 to 20 m*M*. The parameters K_m and V_{max} were calculated by nonlinear fitting to the Michaelis–Menten equation using *Origin* 7.5, whereas the k_{cat} value was derived from

Figure 2
(*a*) The active site of DacB. The side chains of the active-site residues are shown as cyan sticks. Water molecules and zinc ions are shown as red and grey spheres, respectively. Hydrogen bonds and zinc coordination bonds are shown as black and green dashed lines, respectively. The acetate molecule is superimposed on an electron-density map ($2mF_o - DF_c$) contoured at 0.52 e Å^{-3} (1.5σ). (*b*) Active-site comparison of DacB with *Sp*LdcB (lemon; PDB entry 4ox5). The zinc ions in DacB and *Sp*LdcB are shown as grey and lemon spheres, respectively. (*c*) Active-site comparison of DacB with *E. gallinarum* VanXY$_C$ (magenta; PDB entry 4oak). The brown sphere represents the copper ion in VanXY$_C$. (*d*) Surface representation of the substrate-binding pockets of DacB (left) and VanXY$_C$ (right). The β5–α5 loop in DacB and the bisubstrate selectivity loop in VanXY$_C$ are shown as cartoons; the acetate and D-Ala-D-Ala molecules are shown as yellow and magenta sticks, respectively. The active-site pockets are marked by black circles.

V_{max} [k_{cat} = V_{max} (in s^{-1} m*M*)/DacB concentration (in m*M*)]. Three independent assays were performed to calculate the means and standard deviations for all parameters.

The relative enzymatic activities of the DacB mutants were measured using 1 m*M* tetrapeptide (L-Ala-D-iGln-L-Lys-D-Ala) as the substrate. All of the assays were also performed at 37°C in buffer consisting of 100 m*M* Tris–HCl pH 7.5. The reactions were initiated by the addition of 10 n*M* DacB mutant and were terminated by adding 0.1 *M* HCl after 60 min incubation. Three independent assays were performed.

3. Results and discussion

3.1. The overall structure of DacB

The 1.71 Å resolution structure of DacB was determined by the single-wavelength anomalous diffraction phasing method. Structural comparison of the native and SeMet-substituted structures yields a root-mean-square deviation (r.m.s.d.) of 0.247 Å over 175 C^{α} atoms, suggesting that there are no significant differences between the two structures. Thus, we used the native structure in the following analyses. Each asymmetric unit contains three protein molecules, with a largest buried interface area of only 650 $Å^2$, which is not large enough to stabilize a trimer or a dimer. Size-exclusion chromatography also confirmed that DacB exists as a monomer in solution. Each molecule consists of residues Lys54–Val237, lacking the N-terminal 27 residues (Glu27–Lys53) and the last C-terminal residue Asp238 owing to poor electron density. The three molecules in an asymmetric unit are quite similar to each other, with an r.m.s.d. of 0.24–0.28 Å over 184 C^{α} atoms. The major structural differences between the three molecules come from variations in the $\beta5$–$\alpha5$ and $\beta6$–$\alpha6$ loops. Molecule *A* was taken as an example in the structural analyses described here.

The overall structure of DacB adopts a globular fold of the $\alpha+\beta$ class (Fig. 1*a*). The core structure consists of four antiparallel β-strands ($\beta4$–$\beta7$), packed on both sides by several helices ($\alpha1$–$\alpha8$). In addition, DacB has an N-terminal extension consisting of a three-stranded antiparallel β-sheet ($\beta1$–$\beta3$) (Fig. 1*a*). A zinc ion and an acetate molecule were well defined at the centre of the core structure. The atomic

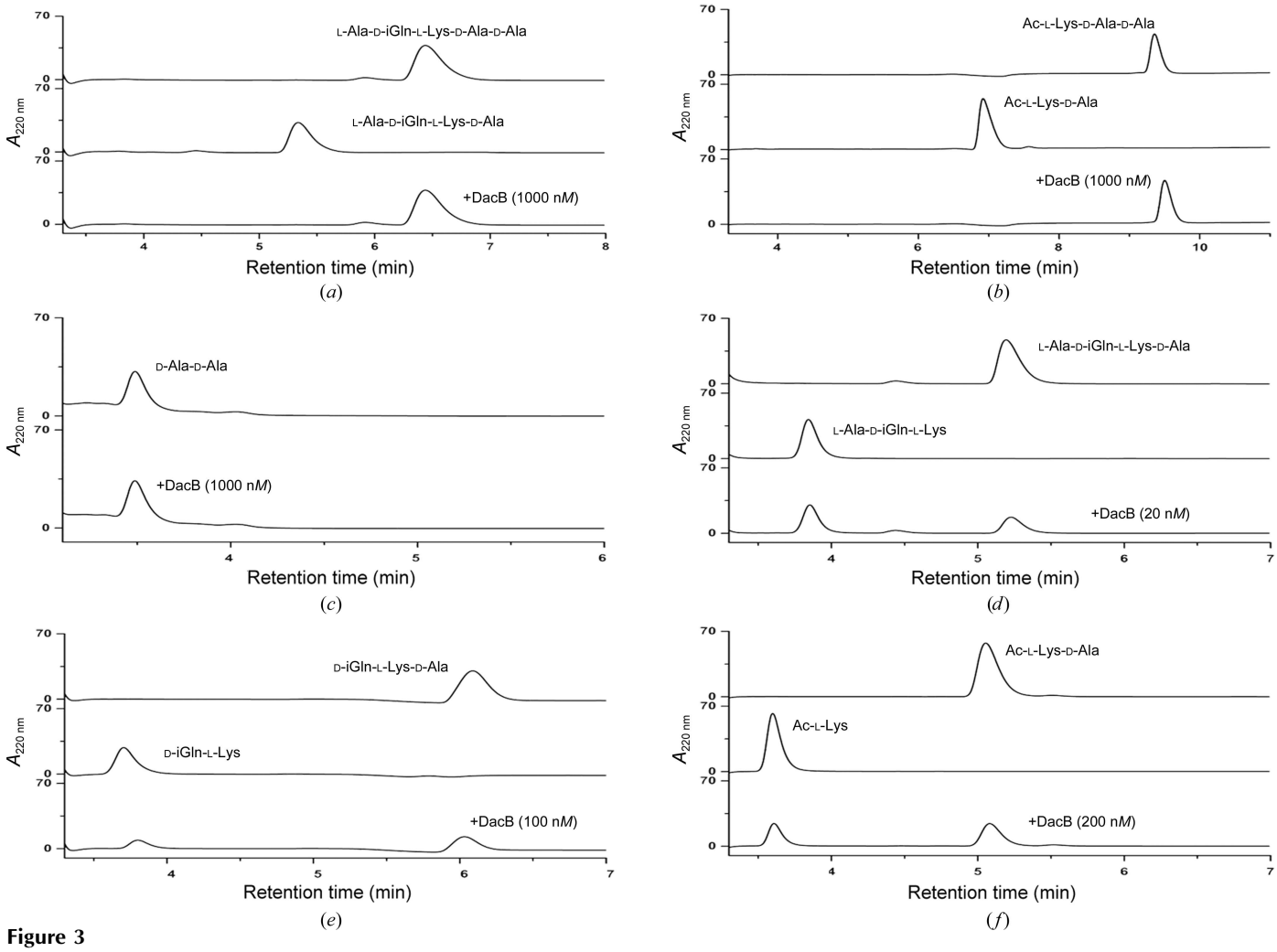

Figure 3
Hydrolytic activity assays of DacB. HPLC profiles towards various peptides: (*a*) L-Ala-D-iGln-L-Lys-D-Ala-D-Ala, (*b*) Ac-L-Lys-D-Ala-D-Ala, (*c*) D-Ala-D-Ala (D-Ala could not be detected by HPLC at 220 nm; therefore, we monitored the decrease in substrate), (*d*) L-Ala-D-iGln-L-Lys-D-Ala, (*e*) D-iGln-L-Lys-D-Ala and (*f*) Ac-L-Lys-D-Ala.

absorption spectrum also confirmed the presence of zinc in DacB at a 1:1 molar ratio.

A *DALI* search (Holm & Rosenström, 2010) revealed that DacB mostly resembles members of the M15B subfamily (Rawlings *et al.*, 2012). The top hits include DacB from *S. pneumoniae* D39 (PDB entry 4d0y; *Z*-score 33.8, r.m.s.d. of 0.7 Å over 183 C^{α} atoms; Abdullah *et al.*, 2014), *Sp*LdcB from *S. pneumoniae* R6 (PDB entry 4ox5; *Z*-score 33.2, r.m.s.d. of 0.8 Å over 182 C^{α} atoms), *Bs*LdcB from *Bacillus subtilis* (PDB entry 4ox3; *Z*-score 20.1, r.m.s.d. of 2.5 Å over 167 C^{α} atoms) and *Ba*LdcB from *B. anthracis* (PDB entry 4mph; *Z*-score 20.3, r.m.s.d. of 2.2 Å over 156 C^{α} atoms; Hoyland *et al.*, 2014). Compared with these recently reported structures, all three of the molecules in our DacB structure could be closely superimposed on the structure of chain *A* of DacB from *S. pneumoniae* D39 (PDB entry 4d0y) and the structure of *Sp*LdcB in complex with D-Ala (PDB entry 4ox5) (Fig. 1*b*), both of which represent a closed conformation (Abdullah *et al.*, 2014; Hoyland *et al.*, 2014). In contrast, the structures of chain *B* of DacB from *S. pneumoniae* D39 (PDB entry 4d0y) and *Sp*LdcB in complex with a product mimic (PDB entry 4oxd) represent an open conformation that is somewhat different from the closed state owing to rearrangement of the $\beta5$–$\alpha5$ loop and the N-terminus of the $\alpha5$ helix surrounding the active site (Fig. 1*c*).

Table 2
Kinetic parameters for DacB.

Substrates	K_m (m*M*)	k_{cat} (s^{-1})	k_{cat}/K_m (s^{-1} mM^{-1})
Ac-L-Lys-D-Ala	6.28 ± 1.22	14.91 ± 0.23	2.37 ± 0.34
D-iGln-L-Lys-D-Ala	7.21 ± 0.98	53.66 ± 0.03	7.62 ± 0.33
L-Ala-D-iGln-L-Lys-D-Ala	2.84 ± 0.37	91.49 ± 0.05	32.14 ± 1.34

The successful hits include the vancomycin-resistance bifunctional D,D-dipeptidase/D,D-carboxypeptidase $VanXY_C$ from *Enterococcus gallinarum* (PDB entry 4oak; *Z*-score 18.3, r.m.s.d. of 2.2 Å over 159 C^{α} atoms) and $VanXY_G$ from *E. faecalis* (PDB entry 4f78; *Z*-score 16.4, r.m.s.d. of 2.4 Å over 159 C^{α} atoms; Meziane-Cherif *et al.*, 2014). Superposition of DacB on $VanXY_C$ reveals that they share a similar core structure but possess highly divergent deletions and/or insertions of structural segments (Fig. 1*d*). Besides these M15B members, DacB also resembles the D-Ala-D-Ala dipeptidase VanX from *E. faecium* (PDB entry 1r44; Bussiere *et al.*, 1998) and the enzymatically active domain (EAD) of the *Listeria bacteriophage* endolysin Ply500 (PDB entry 1xp2; Korndörfer *et al.*, 2008), which belong to the M15D and M15C subfamilies, respectively.

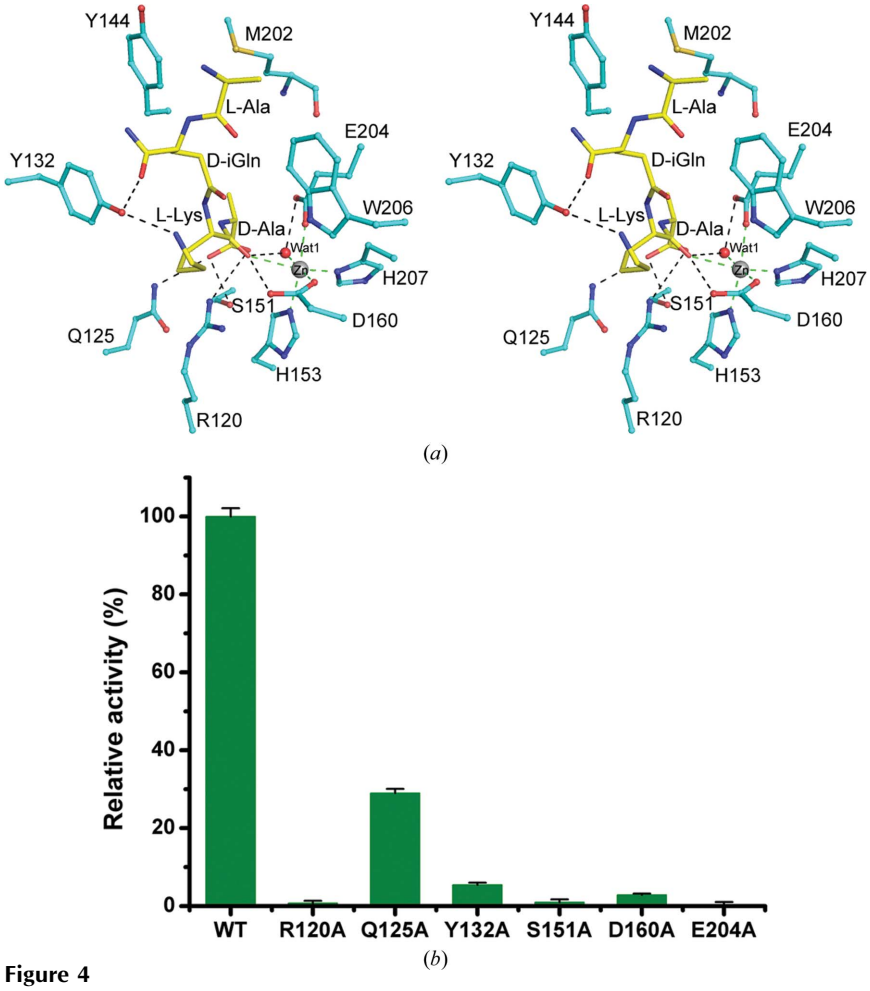

Figure 4
Simulation and validation of the substrate-binding pattern. (*a*) The binding pattern of the tetrapeptide. The tetrapeptide and the binding residues are shown as yellow and cyan sticks, respectively. (*b*) The relative activities of wild-type DacB (WT) and mutants.

3.2. The active site

In the active site of DacB (Fig. 2*a*), a zinc ion is coordinated by six ligands: His153 N^{ε} (2.1 Å), Asp160 $O^{\delta1}$ (2.1 Å), His207 N^{δ} (2.0 Å), Glu204 $O^{\varepsilon1}$ (2.4 Å) and two water molecules Wat1 and Wat2 (2.3 and 2.2 Å, respectively). Glu204 acts as a catalytic base to activate one of the water molecules for nucleophilic attack on the carbonyl C atom of the peptide and then acts as a catalytic acid to protonate the scissile N atom, promoting cleavage of the peptide bond (Bussiere *et al.*, 1998; Matthews *et al.*, 2006). This gives the zinc an octahedral coordination. Adjacent to the zinc, a well defined acetate ion, which was introduced from the crystallization buffer, occupies part of the substrate-binding pocket. The acetate molecule forms hydrogen bonds to Gln125, Ser151, water molecule Wat1 and Arg120, which stabilizes the negative charge at the tetrahedral centre in the transition state (Bussiere *et al.*, 1998; Matthews *et al.*, 2006).

Structural comparison suggested that most active-site residues in DacB are conserved amongst its structural neighbours, and the acetate molecule in DacB occupies a position corresponding to the C-terminus of

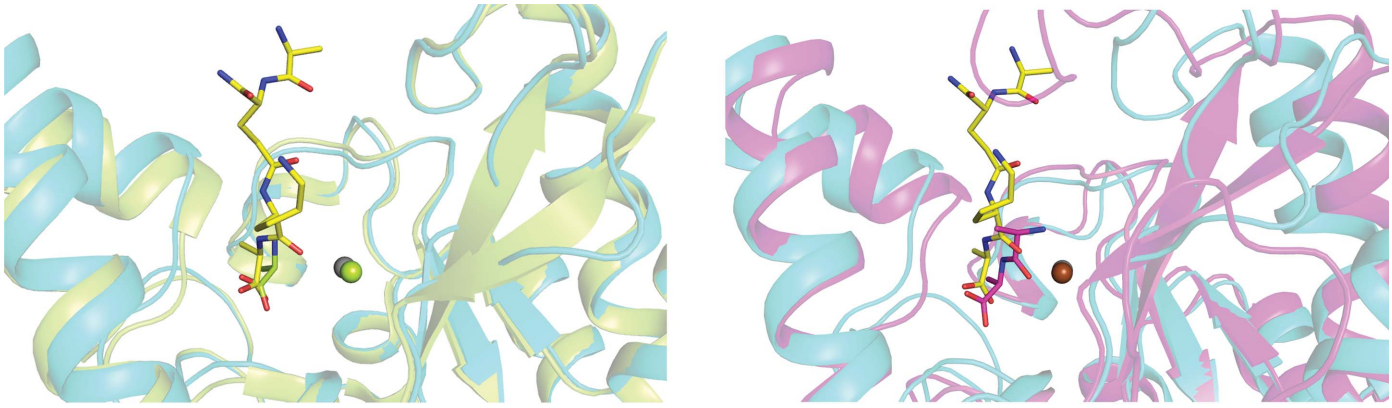

(*a*) (*b*)

Figure 5
Comparison of the DacB docking model with homologues. (*a*) *Sp*LdcB in complex with D-Ala (PDB entry 4ox5). (*b*) VanXY$_C$ in complex with D-Ala-D-Ala (PDB entry 4oak). DacB is shown as a cyan cartoon and other structures are shown as lemon and magenta cartoons, respectively. The tetrapeptide in DacB, the D-Ala in LdcB and the D-Ala-D-Ala in VanXY$_C$ are shown as yellow, lemon and magenta sticks, respectively.

the D-Ala in *Sp*LdcB (Fig. 2*b*) and the D-Ala-D-Ala in VanXY$_C$ (Fig. 2*c*), respectively. Thus, we speculated that the acetate molecule in the active-site pocket of DacB could mimic the carboxyl group of the substrate.

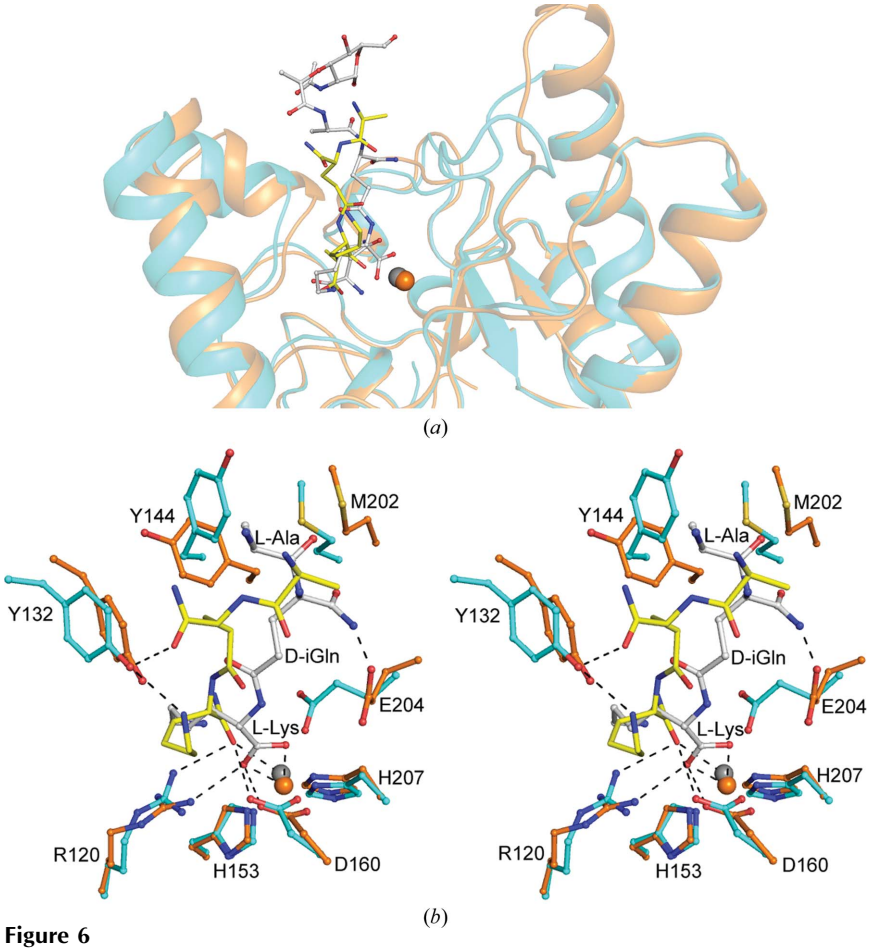

(*a*)

(*b*)

Figure 6
Comparison of our DacB docking model with *Sp*LdcB in complex with MurNAc-L-Ala-D-iGln-L-Lys-(D-Asn) (orange; PDB entry 4oxd). (*a*) The tetrapeptide L-Ala-D-iGln-L-Lys-D-Ala in our DacB structure and the product mimic MurNAc-L-Ala-D-iGln-L-Lys-(D-Asn) in *Sp*LdcB are located in a similar position in the active-site pocket. (*b*) Comparison of the binding patterns of the two ligands. The L-Ala-D-iGln-L-Lys-D-Ala in our complex model and the MurNAc-L-Ala-D-iGln-L-Lys-(D-Asn) in *Sp*LdcB are shown as yellow and grey sticks, respectively.

Unlike the tetrahedral coordination of the zinc ion in the previously reported structures, the zinc ion of DacB is coordinated by six ligands, the extra two of which are contributed by the conserved residue Glu204 and water molecule Wat2 (Fig. 2*a*). Perhaps owing to the absence of substrate, the hexacoordination of zinc in our DacB structure might represent a closed/inactive conformation.

Compared with DacB, the bisubstrate selectivity loop of VanXY$_C$ is seven residues longer than the corresponding $\beta5$–$\alpha5$ loop of DacB, making the active-site pocket of VanXY$_C$ much smaller than that of DacB (Fig. 2*d*). Consequently, the active-site pocket of VanXY$_C$ can perfectly accommodate its favoured dipeptide substrate D-Ala-D-Ala. In VanXY$_C$ residues Leu113 and Ile114 from the bisubstrate selectivity loop and Leu70 and Val87 form a compact hydrophobic pocket to stabilize the methyl group of the N-terminal D-Ala of the substrate (Meziane-Cherif *et al.*, 2014). In contrast, the shorter $\beta5$–$\alpha5$ loop in DacB makes the active-site pocket much larger. This large pocket of DacB surrounded by residues Leu168, Leu128, Tyr132 and Tyr144 is not complementary to a small substrate such as the dipeptide D-Ala-D-Ala (Fig. 2*d*), but matches the peptide stem of L-Ala-D-iGln-L-Lys-D-Ala of PG well.

3.3. Molecular docking of the tetrapeptide

A previous report suggested that DacA and DacB are carboxypeptidases that

sequentially remove the two C-terminal D-Ala residues from PG pentapeptides (Barendt *et al.*, 2011; Abdullah *et al.*, 2014). Recent reports of *in vitro* enzymatic activity of *Sp*LdcB towards the peptidoglycan of *ldc*B-knockout *S. pneumoniae* R6 strain and the synthetic tetrapeptide L-Ala-D-Gln-L-Lys-D-Ala also proved that DacB could remove the C-terminal D-Ala from the tetrapeptide (Hoyland *et al.*, 2014). However, the enzymatic parameters of DacB have not been determined. Here, we checked the *in vitro* activity of recombinant DacB towards a series of *S. pneumoniae* PG stem peptides: the pentapeptide L-Ala-D-iGln-L-Lys-D-Ala-D-Ala, the mono-acetylated tripeptide Ac-L-Lys-D-Ala-D-Ala, the dipeptide D-Ala-D-Ala, the tetrapeptide L-Ala-D-iGln-L-Lys-D-Ala and the tripeptide D-iGln-L-Lys-D-Ala, as well as the mono-acetylated dipeptide Ac-L-Lys-D-Ala. No activity towards the peptides ending in D-Ala-D-Ala (L-Ala-D-iGln-L-Lys-D-Ala-D-Ala, Ac-L-Lys-D-Ala-D-Ala and D-Ala-D-Ala) could be detected (Figs. 3*a*, 3*b* and 3*c*), suggesting that DacB does not act as a D,D-carboxypeptidase. In contrast, DacB could hydrolyze the peptide bond between L-Lys and D-Ala in the peptides ending in L-Lys-D-Ala at various velocities (Figs. 3*d*, 3*e* and 3*f*). The K_m and k_{cat} values of DacB towards the tetrapeptide are 2.84 $\pm$ 0.37 m*M* and 91.49 $\pm$ 0.05 s^{-1}, respectively (Table 2), giving an activity (k_{cat}/K_m) of 32.14 $\pm$ 1.34 mM^{-1} s^{-1}, which is over four times that for the tripeptide and about 15 times that for the mono-acetylated dipeptide, respectively (Table 2). These results clearly demonstrate that DacB indeed acts as an L,D-carboxypeptidase towards the natural substrate, the tetrapeptide L-Ala-D-iGln-L-Lys-D-Ala of *S. pneumoniae* PG, which is in agreement with the recently reported results (Abdullah *et al.*, 2014; Hoyland *et al.*, 2014).

To understand tetrapeptide binding by DacB, we attempted to crystallize DacB in the presence of the tetrapeptide, but failed. Alternatively, we docked the tetrapeptide into DacB using *AutoDock Vina* (Trott & Olson, 2010). The output gave nine binding states and we chose the model that best matched the terminal carboxylate of the peptide to the position of the acetate in the crystal structure reported here. Residues Arg120, Gln125 and Ser151 of DacB form hydrogen bonds to the carboxyl group of the tetrapeptide, forming a network of interactions similar to that observed involving the acetate molecule in our DacB structure (Fig. 4*a*) and the corresponding D-Ala residue in either *Sp*LdcB (PDB entry 4ox5) or $VanXY_C$ (PDB entry 4oak) (Fig. 5). The main-chain O atom of the L-Lys residue directly interacts with the zinc ion, while its side chain points outwards and is fixed by Tyr132, which also stabilizes the D-iGln residue. Although the N-terminal L-Ala makes no polar interactions with the active-site pocket, it forms hydrophobic interactions with three residues Tyr144, Met202 and Trp206. Thus, the N-terminal L-Ala is also important for substrate recognition, which is consistent with the enzymatic assays (Table 2). Notably, the N-terminal L-Ala of the tetrapeptide that is covalently linked to the PG glycan chains protrudes out of the pocket. Thus, the large active-site pocket of DacB might also accommodate the PG glycan chains of its natural substrate.

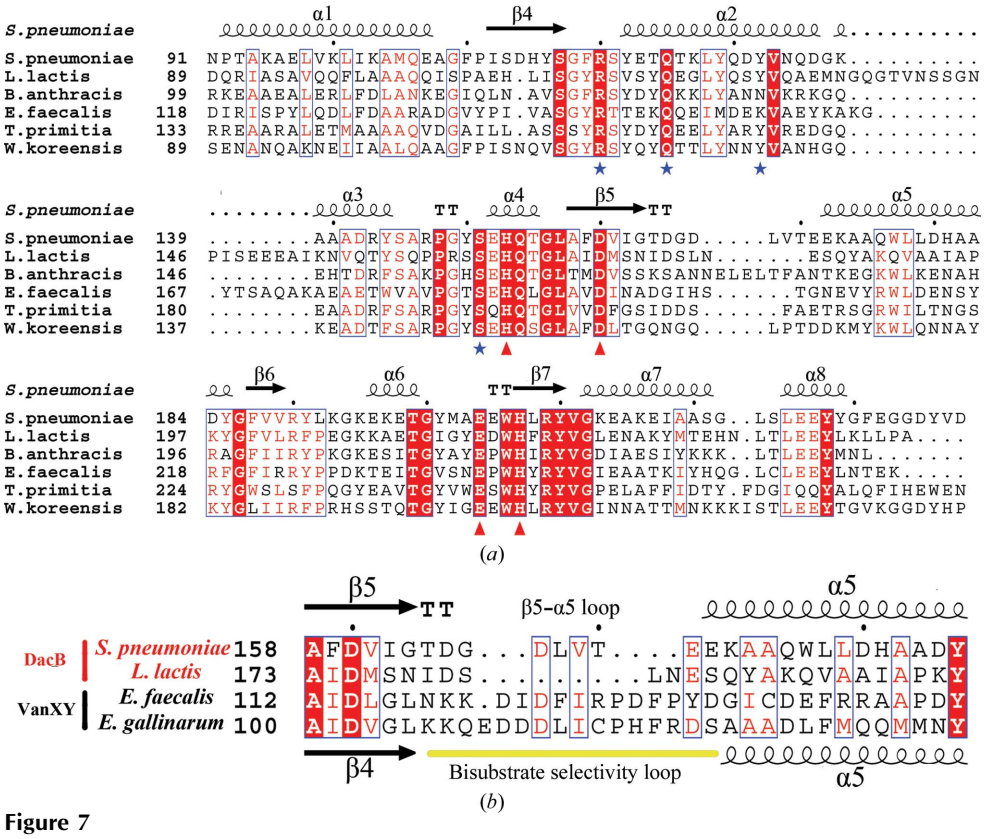

Figure 7
Structure-based sequence alignment of M15B subfamily peptidases. (*a*) The residues involved in zinc and substrate binding are conserved. The substrate-binding residues are indicated by blue stars and the zinc-binding residues are marked with red triangles. (*b*) The characterized DacB enzymes lack the bisubstrate selectivity loop found in VanXY enzymes.

Superposition of the docking model on the structure of *Sp*LdcB in complex with MurNAc-L-Ala-D-iGln-L-Lys-(D-Asn; PDB entry 4oxd) revealed that the tetrapeptide L-Ala-D-iGln-L-Lys-D-Ala in DacB and the product mimic MurNAc-L-Ala-D-iGln-L-Lys-(D-Asn) in *Sp*LdcB are located in similar positions (Fig. 6*a*). We compared the binding modes of the shared L-Ala-D-iGln-L-Lys moiety in the two ligands (Fig. 6*b*). Although the L-Ala moieties of the two ligands adopt a somewhat different conformation, they both interact with Tyr144 and Met202. The amide groups of D-iGln in the two ligands point in opposite directions and form hydrogen bonds to Glu204 (*Sp*LdcB) and Tyr132 (DacB), respectively. The L-Lys side chain in *Sp*LdcB

projects into the inner core, whereas it points outwards in our model of the DacB complex. However, the main-chain O atoms of L-Lys in both ligands interact with the zinc ion and Arg120.

To validate the docking model, we subsequently performed site-directed mutagenesis in combination with activity assays (Fig. 4*b*). The E204A mutation almost completely abolishes the peptidase activity, implying that Glu204 is indispensable for catalysis. The D160A mutation also leads to a loss of enzymatic activity, suggesting that the zinc-coordinating residue Asp160 is crucial for catalysis. The single mutations R120A, S151A or Y132A caused an almost complete loss of enzymatic activity, indicating their roles in stabilizing the tetrapeptide. In contrast, the Q125A mutant still retains approximately 30% activity, indicating that Gln125 is involved in, but is not crucial for, substrate binding. Multiple sequence alignment (Fig. 7*a*) revealed that these residues are highly conserved in DacB homologues from Gram-positive bacteria. Interestingly, both of the two characterized L,D-carboxypeptidases lack the bisubstrate selectivity loop found in VanXY enzymes (Fig. 7*b*), suggesting that these enzymes might present an open architecture of the active site to accommodate larger PG fragments ending in L-Lys-D-Ala.

S. pneumoniae infections have been successfully treated using the classic β-lactam antibiotics, which inhibit some PG synthetases, such as PBPs (Hakenbeck *et al.*, 1999). However, the worldwide increase in multidrug-resistant strains is an emergent medical and social issue, as 25% of all invasive *S. pneumoniae* strains are resistant to penicillin (Pallares *et al.*, 1998). Therefore, it is important to develop novel drugs against other PG hydrolases. Our study presents structural and biochemical analyses of DacB from *S. pneumoniae*. Enzymatic activity assays showed that DacB is an L,D-carboxypeptidase towards the tetrapeptide L-Ala-D-iGln-L-Lys-D-Ala, which was further docked into our DacB structure. Thus, our structure gives hints for the design of possible DacB inhibitors derived from the tetrapeptide and/or its analogues.

We thank the staff at the Shanghai Synchrotron Radiation Facility for technical assistance. This work was supported by the Ministry of Science and Technology of China (Grant Nos. 2014CB910100 and 2013CB835300) and the National Natural Science Foundation of China (Grant No. 31270781).

References

Abdullah, M. R., Gutiérrez-Fernández, J., Pribyl, T., Gisch, N., Saleh, M., Rohde, M., Petruschka, L., Burchhardt, G., Schwudke, D., Hermoso, J. A. & Hammerschmidt, S. (2014). *Mol. Microbiol.* **93**, 1183–1206.

Adams, P. D. *et al.* (2010). *Acta Cryst.* D**66**, 213–221.

Afonine, P. V., Grosse-Kunstleve, R. W., Echols, N., Headd, J. J., Moriarty, N. W., Mustyakimov, M., Terwilliger, T. C., Urzhumtsev, A., Zwart, P. H. & Adams, P. D. (2012). *Acta Cryst.* D**68**, 352–367.

Barendt, S. M., Sham, L. T. & Winkler, M. E. (2011). *J. Bacteriol.* **193**, 2290–2300.

Brodersen, D. E., de La Fortelle, E., Vonrhein, C., Bricogne, G., Nyborg, J. & Kjeldgaard, M. (2000). *Acta Cryst.* D**56**, 431–441.

Bussiere, D. E., Pratt, S. D., Katz, L., Severin, J. M., Holzman, T. & Park, C. H. (1998). *Mol. Cell*, **2**, 75–84.

Chen, V. B., Arendall, W. B., Headd, J. J., Keedy, D. A., Immormino, R. M., Kapral, G. J., Murray, L. W., Richardson, J. S. & Richardson, D. C. (2010). *Acta Cryst.* D**66**, 12–21.

Cowtan, K. (2006). *Acta Cryst.* D**62**, 1002–1011.

Emsley, P. & Cowtan, K. (2004). *Acta Cryst.* D**60**, 2126–2132.

Engh, R. A. & Huber, R. (1991). *Acta Cryst.* A**47**, 392–400.

Hakenbeck, R., Grebe, T., Zähner, D. & Stock, J. B. (1999). *Mol. Microbiol.* **33**, 673–678.

Hakenbeck, R. & Kohiyama, M. (1982). *Eur. J. Biochem.* **127**, 231–236.

Heijenoort, J. van (2011). *Microbiol. Mol. Biol. Rev.* **75**, 636–663.

Holm, L. & Rosenström, P. (2010). *Nucleic Acids Res.* **38**, W545–W549.

Hoyland, C. N., Aldridge, C., Cleverley, R. M., Duchêne, M.-C., Minasov, G., Onopriyenko, O., Sidiq, K., Stogios, P. J., Anderson, W. F., Daniel, R. A., Savchenko, A., Vollmer, W. & Lewis, R. J. (2014). *Structure*, **22**, 949–960.

Korndörfer, I. P., Kanitz, A., Danzer, J., Zimmer, M., Loessner, M. J. & Skerra, A. (2008). *Acta Cryst.* D**64**, 644–650.

Laskowski, R. A., MacArthur, M. W., Moss, D. S. & Thornton, J. M. (1993). *J. Appl. Cryst.* **26**, 283–291.

Massidda, O., Nováková, L. & Vollmer, W. (2013). *Environ. Microbiol.* **15**, 3133–3157.

Matthews, M. L., Periyannan, G., Hajdin, C., Sidgel, T. K., Bennett, B. & Crowder, M. W. (2006). *J. Am. Chem. Soc.* **128**, 13050–13051.

Meziane-Cherif, D., Stogios, P. J., Evdokimova, E., Savchenko, A. & Courvalin, P. (2014). *Proc. Natl Acad. Sci. USA*, **111**, 5872–5877.

Morlot, C., Noirclerc-Savoye, M., Zapun, A., Dideberg, O. & Vernet, T. (2004). *Mol. Microbiol.* **51**, 1641–1648.

Morlot, C., Pernot, L., Le Gouellec, A., Di Guilmi, A. M., Vernet, T., Dideberg, O. & Dessen, A. (2005). *J. Biol. Chem.* **280**, 15984–15991.

Morris, G. M., Huey, R., Lindstrom, W., Sanner, M. F., Belew, R. K., Goodsell, D. S. & Olson, A. J. (2009). *J. Comput. Chem.* **30**, 2785–2791.

Murshudov, G. N., Skubák, P., Lebedev, A. A., Pannu, N. S., Steiner, R. A., Nicholls, R. A., Winn, M. D., Long, F. & Vagin, A. A. (2011). *Acta Cryst.* D**67**, 355–367.

Otwinowski, Z. & Minor, W. (1997). *Methods Enzymol.* **276**, 307–326.

Pallares, R., Viladrich, P. F., Liñares, J., Cabellos, C. & Gudiol, F. (1998). *Microb. Drug Resist.* **4**, 339–347.

Rawlings, N. D., Barrett, A. J. & Bateman, A. (2012). *Nucleic Acids Res.* **40**, D343–D350.

Scheffers, D. J. & Pinho, M. G. (2005). *Microbiol. Mol. Biol. Rev.* **69**, 585–607.

Schuster, C., Dobrinski, B. & Hakenbeck, R. (1990). *J. Bacteriol.* **172**, 6499–6505.

Severin, A., Schuster, C., Hakenbeck, R. & Tomasz, A. (1992). *J. Bacteriol.* **174**, 5152–5155.

Sham, L.-T., Tsui, H.-C. T., Land, A. D., Barendt, S. M. & Winkler, M. E. (2012). *Curr. Opin. Microbiol.* **15**, 194–203.

Smith, T. J., Blackman, S. A. & Foster, S. J. (2000). *Microbiology*, **146**, 249–262.

Trott, O. & Olson, A. J. (2010). *J. Comput. Chem.* **31**, 455–461.

Vagin, A. & Teplyakov, A. (2010). *Acta Cryst.* D**66**, 22–25.

Vollmer, W., Blanot, D. & de Pedro, M. A. (2008). *FEMS Microbiol. Rev.* **32**, 149–167.

Vollmer, W., Joris, B., Charlier, P. & Foster, S. (2008). *FEMS Microbiol. Rev.* **32**, 259–286.

Winn, M. D. *et al.* (2011). *Acta Cryst.* D**67**, 235–242.

Wyckoff, T. J., Taylor, J. A. & Salama, N. R. (2012). *Trends Microbiol.* **20**, 540–547.

Zapun, A., Vernet, T. & Pinho, M. G. (2008). *FEMS Microbiol. Rev.* **32**, 345–360.